



HAL
open science

Fast terminal sliding mode control-based direct power control for single-stage single-phase PV system

Elaheh Heydari, Ali Yazdian Varjani, Demba Diallo

► **To cite this version:**

Elaheh Heydari, Ali Yazdian Varjani, Demba Diallo. Fast terminal sliding mode control-based direct power control for single-stage single-phase PV system. *Control Engineering Practice*, 2020, 104, pp.104635. 10.1016/j.conengprac.2020.104635 . hal-03491413

HAL Id: hal-03491413

<https://hal.science/hal-03491413>

Submitted on 21 Sep 2022

HAL is a multi-disciplinary open access archive for the deposit and dissemination of scientific research documents, whether they are published or not. The documents may come from teaching and research institutions in France or abroad, or from public or private research centers.

L'archive ouverte pluridisciplinaire **HAL**, est destinée au dépôt et à la diffusion de documents scientifiques de niveau recherche, publiés ou non, émanant des établissements d'enseignement et de recherche français ou étrangers, des laboratoires publics ou privés.



Distributed under a Creative Commons Attribution - NonCommercial 4.0 International License

Fast terminal sliding mode control- based direct power control for single-stage single-phase PV system

Elaheh Heydari^{1,2}, Ali Yazdian Varjani¹, Demba Diallo²

¹Department of Electrical Engineering, Tarbiat Modares University, Tehran, Iran

²Universite Paris-Saclay, CentraleSupélec, CNRS, GeePs, Sorbonne Université, 91192 Gif/Yvette, France

Abstract

Today, grid-connected photovoltaic systems have gained widespread penetration among renewable energy systems. For low power applications, a single-phase inverter with less power converter is a good compromise for high efficiency. The control must make it possible to extract the maximum power from the photovoltaic modules, ensure good dynamic performance for active and reactive power injection, ensure power quality, and reject disturbances and parameter mismatch. Besides, the controllers of the grid and PV sides should be coordinated. In this study, a fast terminal sliding mode control combined with Direct Power Control is proposed. Thanks to the two-cascaded control loops, simulations and experimental results with a 1-kW test bench have proven the proposal's effectiveness in terms of dynamic performances and robustness to irradiance variations. Comparison with deadbeat-Direct Power Control, predictive control, and power hysteresis control shows that our proposal leads to lower Total Harmonic Distortion (3,5%) for the electrical grid's current and lower time response (one-tenth of half the grid cycle).

Keywords: single-phase single-stage PV inverter; direct power control (DPC); fast terminal sliding mode control (FTSMC).

Nomenclature

V_g (V)	Grid voltage
V_{inv} (V)	Inverter voltage
I_g (A)	Grid current
f_o (Hz)	Grid frequency
f_{sw} (Hz)	Switching frequency
$f_{sampling}$ (Hz)	Sampling frequency
L (H)	Filter inductance
R (Ω)	Filter resistance
PV	Photovoltaic
MPPT	Maximum Power Point Tracking
P&O	Perturb and Observe
IC	Incremental Conductance
DPC	Direct Power Control
SMC	Sliding Mode Control
FTSMC	Fast Terminal Sliding Mode Control
SPWM	Sinusoidal Pulse Width Modulation
THD	Total Harmonic Distortion

1. Introduction

Because of environmental issues, renewables are expected to be the fastest-growing energy source for electricity production. Its contribution is expected in 2025 to be double its value in 2008 [1]. The produced power from the renewables has increased and has shifted from stand-

alone to grid-connected as the technologies of power electronic converters and control methods are becoming more mature [2]. Among Renewable energy sources (RES), photovoltaic (PV) plants have experienced the fastest growth thanks to the progress in semiconductor materials, in packaging, and cost reduction.

The connection of the PV power plant to the grid can be made with single or two-stage power converters [3].

In the two-stage case, the PV power plant is connected to the grid through a DC-DC converter, followed by an inverter. One of the main advantages of this structure is the reduction of the power converters' current rating, thanks to the higher DC bus voltage. However, with this double stage power conversion, the efficiency is lower and the cost is higher when compared to a single stage power conversion [4].

The single-phase interface composed of a voltage inverter is usually adopted to connect low power PV plant to the grid. An important issue is the control of the power converter with two main objectives; regulate the injected power to the grid with the lowest harmonic distortion and high dynamic performances. The control is done through two control loops [4]. The inner loop generates the power switching signals to modulate the inverter output current in accordance with the grid requirements. The outer loop uses maximum power point tracking (MPPT) algorithms such as Perturb and Observe (P&O) or Incremental Conductance (IC) to capture the maximum power from the solar panels [5-8].

Among the different control techniques that have been explored for the control of grid-tied power converters [9-12], Direct Power Control (DPC) is particularly of interest. It has been used in three-phase grid side converters for the control of active filters and wind turbines [13, 14]. It

has also been used for the control of active and reactive power in a single-phase grid side converter [15]. Its popularity is due to its simplicity and ease of digital implementation. However, it suffers from low robustness to model parameter mismatches, low dynamic performance and low grid current quality. Sliding Mode Control (SMC) is a control method robust against parameter variations and model mismatches [16]. It exhibits also good dynamic performances due to its inherent switching nature [17, 18]. However, the conventional SMC suffers from poor transient response during grid voltage distortions [19]. This issue can be addressed with higher coefficient on the sliding surface but to the detriment of a low convergence rate. The fast terminal sliding mode control (FTSMC) proves its efficiency in mitigating grid voltage distortions while increasing the convergence rate [20-22]. Finally, we have adopted in this paper a hybrid control method combining fast terminal sliding mode control (FTSMC) and direct power control (DPC) for the control of a single-stage single-phase PV power system.

The rest of the paper is organized as follows. In section 2, the overall system is presented. In section 3, the proposed controller and its design are presented. The simulation and experimental results are described in section 4.

2. System description

The schematic of the single-stage single-phase PV system is depicted in figure 1. The outer control loop sampled at a low frequency implements the Maximum Power Point Tracking (MPPT) using the Perturb and Observe (P&O) algorithm [23]. Its output is the active power reference P_{oref} , and reactive power reference Q_{oref} is set at 0 to operate at a unit power factor.

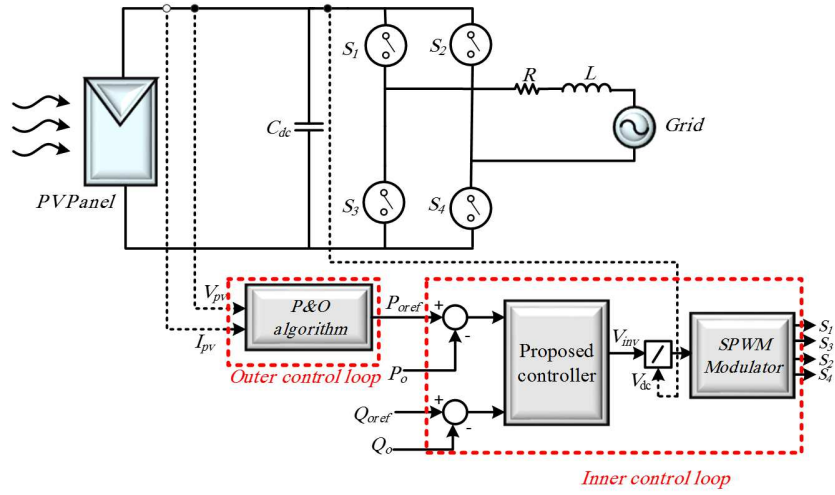


Figure 1. The general structure of the system

The inner control loop is based on a Sinusoidal Pulse Width Modulator (SPWM) to produce the converter switching signals. Its sampling frequency is set higher enough (compared to the grid fundamental frequency). Therefore, the output voltage of the inverter can be assumed equal to its fundamental component. As a consequence, the equivalent circuit in the stationary reference frame ($\alpha\beta$) is displayed in figure 2.

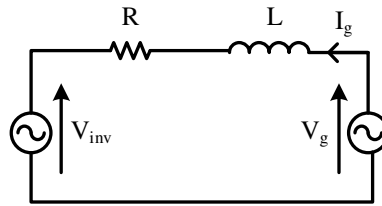


Figure 2. The Equivalent circuit of single-phase grid-tied inverter.

Based on Figure 2, the voltage equation can be written as:

$$V_{g\alpha\beta} = RI_{g\alpha\beta} + L \frac{dI_{g\alpha\beta}}{dt} + V_{inv\alpha\beta} \quad (1)$$

Where R and L are the electrical grid line parameters, $V_{g\alpha\beta}$ is the grid voltage and $V_{inv\alpha\beta}$ is the averaged output voltage of the inverter.

The complex apparent, active power and reactive powers can be computed as:

$$S_o = -\frac{1}{2}V_{g\alpha\beta}I_{g\alpha\beta}^*$$

$$P_o = -\frac{1}{2}(v_{g\alpha}i_{g\alpha} + v_{g\beta}i_{g\beta}) \quad (2)$$

$$Q_o = -\frac{1}{2}(v_{g\beta}i_{g\alpha} - v_{g\alpha}i_{g\beta})$$

where $(x)^*$ stands for the imaginary part. $v_{g\alpha}, v_{g\beta}, i_{g\alpha}, i_{g\beta}$ are the grid voltage and current components in the $(\alpha\beta)$ stationary reference frame, respectively. A phase-locked loop (PLL) and a phase detector are used to obtain these components from the measurements. Second-order-generalised-integrator (SOGI) is adopted to retrieve stationary components [24]. The corresponding transfer functions are expressed as follows:

$$G_d(s) = \frac{x_\alpha}{x} = \frac{k\omega_o s}{s^2 + k\omega_o s + \omega_o^2} \quad (3)$$

$$G_q(s) = \frac{x_\beta}{x} = \frac{k\omega_o^2}{s^2 + k\omega_o s + \omega_o^2}$$

Where k allows tuning the closed-loop system bandwidth and ω_o is the fundamental angular frequency. Equation (3) is applied to the electrical grid current and voltage to obtain the orthogonal two-phase system.

3. Power Control Strategy

A- Fast Terminal Sliding Mode Control

The objective is to minimize the error between the reference powers (active and reactive), and their actual values despite the disturbances, the unavoidable parameter mismatch and the modelling errors.

Sliding mode Control (SMC) is a well-known method popular for the robust control of non-linear systems [25]. The design requires selecting a sliding surface, setting the control law, and finally assessing the stability.

Adding the integral of the error to design the surface helps to reduce the steady-state error and to mitigate the chattering phenomenon. For the conventional SMC, the sliding surface is expressed as:

$$S_s = \left(\frac{d}{dt} + \lambda\right)X_1 \quad (4)$$

Where $X_1 = \int e(\tau)d\tau$, $e(t)$ is the output power error and λ is a time-invariant coefficient.

The solution of (4) in steady-state is expressed as: $X_1(t) = X_1(t_0)e^{-\lambda t}$. Therefore as X_1 represents the error, the convergence time is infinite. Increasing the coefficient may improve the transient but to the detriment of more chattering and will not prevent from the steady-state error. To address this issue terminal sliding mode control (TSMC) has been proposed as an alternative [19].

The sliding surface is defined as:

$$S_{TSMC} = \dot{X}_1 + \delta X_1^{\frac{r}{l}} \quad (5)$$

where r, l are positive odd integers, and δ is a positive integer. In this case, X_1 will reach its equilibrium point in a finite adjustable time expressed as:

$$t_s^{TSMC} = \frac{l}{\delta(l-r)} |X_1(t_0)|^{(1-\frac{r}{l})} \text{ under the condition that } l > r. \text{ This equation shows that the}$$

equilibrium point is reached in finite time. However, it is noticeable that the convergence time depends on the value of the initial point. Fast Terminal SMC is designed to address this issue. With this approach, the sliding surface defined with a linear term and a nonlinear term leads to fast dynamic response whatever the initial point. The sliding surface is now defined as:

$$S_{FTSMC} = \dot{X}_1 + \delta X_1^{\frac{r}{l}} + \gamma X_1 \quad (6)$$

Where γ is a positive integer bringing in an additional linear term.

The expression of the convergence time is as follows:

$$t_s^{FTSMC} = \frac{l}{\delta(l-r)} (\ln(\gamma X_1(t_0)^{(1-\frac{r}{l})} + \delta) - \ln \delta) \text{ under the condition that } l > r.$$

With FTSMC and selecting sliding surface as in (6) the dynamic of the system when the states of the system are not near the equilibrium point ($|X_1| > 1$) is obtained as $\dot{X}_1 = -\gamma X_1$ and when the states of the system are in a close range of the equilibrium point ($|X_1| < 1$) the dynamic is obtained as $\dot{X}_1 = -\delta X_1^{\frac{r}{l}}$.

In both cases, fast dynamic response is obtained [24].

B- Application of FTSMC to Direct Power Control

1- Definition of the sliding surfaces

If we define $e_p = P_{oref} - P_o, e_q = Q_{oref} - Q_o$ the sliding surfaces for the active and reactive powers can be written as:

$$S_t = [S_{ip} \quad S_{iq}]^T$$

$$S_{ip} = e_p(t) + \gamma_p \int e_p(\tau) d\tau + \delta_p \left(\int e_p(\tau) d\tau \right)^{\frac{r}{l}}$$

$$S_{iq} = e_q(t) + \gamma_q \int e_q(\tau) d\tau + \delta_q \left(\int e_q(\tau) d\tau \right)^{\frac{r}{l}} \quad (7)$$

where $(.)^T$ is the transpose operator.

2- Derivation of the control law

The control law is composed of two terms: the equivalent control law $V_{invt(eq)}$ obtained by setting $\dot{S}_t = 0$, and the discontinuous or switching control law $V_{invt(sw)}$ designed to compensate the disturbances that deviate the states from the sliding surface. Finally $V_{invt} = V_{invt(eq)} + V_{invt(sw)}$.

The derivatives of the active and reactive powers are expressed as follows:

$$\frac{dP_o}{dt} = -\frac{1}{2L} [(v_{g\alpha}^2 + v_{g\beta}^2) - (v_{g\alpha} v_{inv\alpha} + v_{g\beta} v_{inv\beta})] - \frac{R}{L} P_o - \omega_o Q_o$$

(8)

$$\frac{dQ_o}{dt} = -\frac{1}{2L} [-v_{g\beta} v_{inv\alpha} - v_{g\alpha} v_{inv\beta}] - \frac{R}{L} Q_o + \omega_o P_o$$

The derivative \dot{S}_t is retrieved from (2) and (8). It can be written as:

$$\dot{S}_t = A_t + B_t V_{invt},$$

$$A_t = [A_{tp} \quad A_{tQ}]^T, B_t = \frac{-1}{2L} \begin{bmatrix} v_{g\alpha} & v_{g\beta} \\ v_{g\beta} & -v_{g\alpha} \end{bmatrix}$$

$$A_{tp} = \frac{R}{L} P_o + \omega_o Q_o + \frac{1}{2L} (v_{g\alpha}^2 + v_{g\beta}^2) + \gamma_p (P_{oref} - P_o) + \frac{r}{l} \delta_p \left(\int (P_{oref} - P_o) d\tau \right)^{r-1} (P_{oref} - P_o)$$

$$A_{tQ} = \frac{R}{L} Q_o - \omega_o P_o + \gamma_q (Q_{oref} - Q_o) + \frac{r}{l} \delta_q \left(\int (Q_{oref} - Q_o) d\tau \right)^{r-1} (Q_{oref} - Q_o) \quad (9)$$

Setting $\dot{S}_t = 0$ allows determining the equivalent control law $V_{invt(eq)} = -B_t^{-1} A_t$.

In order to cope with the disturbances, the additional term that is the switching control law is set

$$\text{as } V_{invt(sw)} = k_t \text{sign}(S_t) = \begin{bmatrix} k_1 & 0 \\ 0 & k_2 \end{bmatrix} \begin{bmatrix} \text{sign}(S_{tp}) \\ \text{sign}(S_{tQ}) \end{bmatrix} \text{ where } k_1, k_2 \text{ are positive coefficients.}$$

The final control law $V_{invt} = V_{invt(eq)} + V_{invt(sw)}$ is applied to the sinusoidal pulse width modulator to determine the inverter's gate signals.

One can notice from (9) that we have at our disposal the adjustable coefficients to minimize the steady-state error and improve the dynamic performances.

Let us remind that the maximum power point tracking (MPPT) algorithm calculates the active power reference while the reactive power reference can be set to zero. The block diagram of the proposed controller is shown in figure 3.

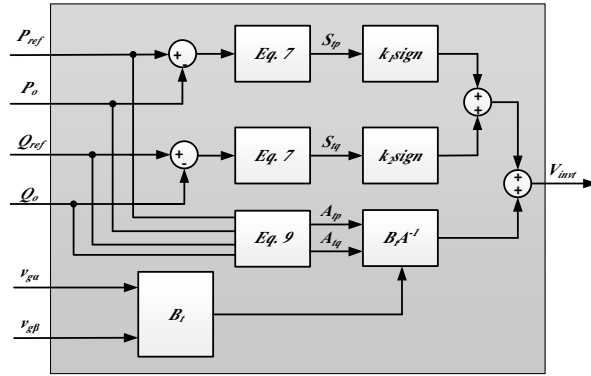


Figure 3. The block diagram of the proposed FTSMC

3- Stability Analysis

It is essential to evaluate the stability of the control law once the states are attracted to the sliding surface. This is done with the help of Lyapunov theorem on stability. The Lyapunov function, in our case is defined as $V_t = \frac{1}{2} S_t^T S_t$. The stability is guaranteed if the condition $\dot{V}_t = S_t^T \dot{S}_t < 0$ is satisfied.

From (7), the following stability condition is derived:

$$\dot{V}_t = S_t^T \dot{S}_t = -k_t S_t^T \text{sign}(S_t) < 0 \quad (10)$$

As $k_t > 0$, the system is stable if $S_t^T \text{sign}(S_t) > 0$.

4- Parameters selection

The parameters used in the definition of the sliding surface (7) must be set to obtain good dynamic performances such as minimum settling time and steady-state error. The parameters r, l are odd integers and must be set to avoid singularity, meaning that $S_t \rightarrow 0$ while the control variable must be bounded. Based on a recursive procedure [21], the minimum values r, l are set as:

$r = 3$, and $l = 5$. The parameters $\gamma_{p,q}, \delta_{p,q}$ must be set at the highest values to reduce the settling time. In the following, they are set at $\gamma_{p,q} = 10000$ and $\delta_{p,q} = 10000$. The last parameters to be set are the coefficients in k_t . They must be set to reject the disturbances within the system efficiently without increasing the inherent chattering phenomenon [26].

Let us define the disturbances as $D = [D_p \ D_q]^T$. If we include the disturbance in the derivative of the sliding surface defined in (9), $\dot{S}_t = A_t + B_t U + D$ and the stability condition becomes:

$$\dot{V}_t = S_t^T \dot{S}_t = S_t^T D - k_t S_t^T \text{sign}(S_t) < 0 \quad (11)$$

The following condition must be respected to guarantee the system's stability on the sliding surface:

$$k_t > D .$$

Once the designer has estimated the disturbances affecting the active and reactive powers, he can tune his switching control coefficients appropriately.

4. Results and Discussions

1- Simulation results

At first, to evaluate our proposal, we have simulated with Matlab-Simulink a single-stage single-phase grid-connected PV system displayed in figure 4. The system parameters are listed in Table 1. It is composed of a PV array model with parameters listed in Table 2, a single-phase inverter, a 110V-220V transformer, and an inductance. The latter has been selected, as recommended in

[27]. Because of using the transformer, grid current (i_g), filter inductance (L), and resistance (R) are moved to the inverter side. So, they have been defined, as i_L, L_f, R_f . The parameters of the controller are listed in Table 3. They have been set, as explained in the previous section.

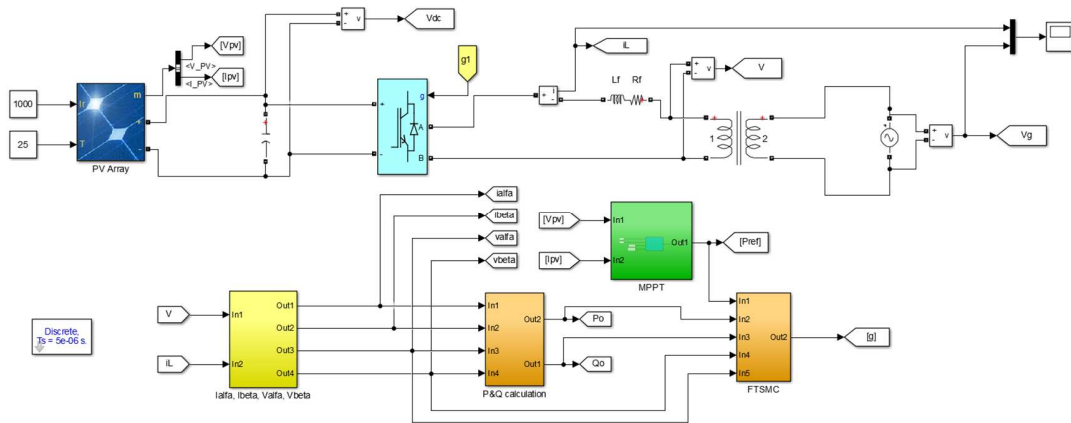


Figure 4. The simulated system in Matlab-Simulink

Table 1. The system parameters.

Parameter	Description	Value
V_g (V)	Grid voltage	220 (RMS)
f_o (Hz)	Grid frequency	50
f_{sw} (kHz)	Switching frequency	6
$f_{sampling}$ (kHz)	Sampling frequency	12
L_f (mH)	Filter inductance	3.25
R_f (m Ω)	Filter resistance	10

Table 2. Specifications of PV module (APOS Energy AP210)

Parameter	Description	Value
P_{MPP} (W)	Maximum PV power	209.85
I_{MPP} (A)	Current at maximum power	7.33

V_{MPP} (V)	Voltage at maximum power	28.63
I_{sc} (A)	Short circuit current	7.79
V_{oc} (V)	Open circuit voltage	36.55
n_s	Series-connected modules per string	7
n_p	Parallel strings	1

Table 3. The proposed controller parameters.

Parameter	Value
k_1, k_2	5000
$\frac{r}{l}$	0.6
Control coefficients: $\gamma_p, \gamma_q, \delta_p, \delta_q$	10000

The Fast Terminal Sliding Mode Control – Direct Power Control (FTSMC-DPC) strategy is evaluated first in a steady-state. The reference of the active power is obtained from MPPT under 1000 W/m^2 solar radiation and 25°C . The reference of the reactive power is set to 0 kVAR. The simulation results are shown in figures 5 and 6. In figure 5 from top to bottom, one can see that the active and reactive powers are perfectly controlled. The last two waveforms represent the electrical grid's voltage and current. In figure 6, the electrical grid's current spectrum is plotted. The THD is equal to 2.97%, which copes with the international standard IEC62040-3 that recommends a $\text{THD} < 5\%$.

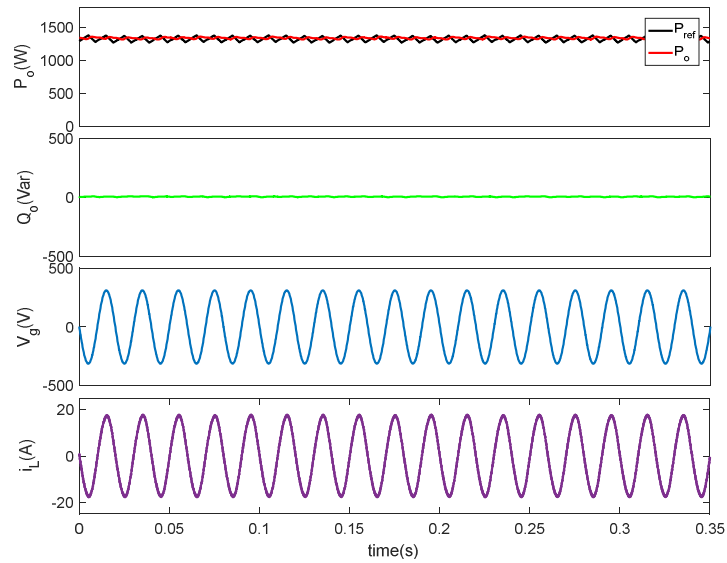


Figure 5. Simulation results of the FTSMC in steady-state condition.

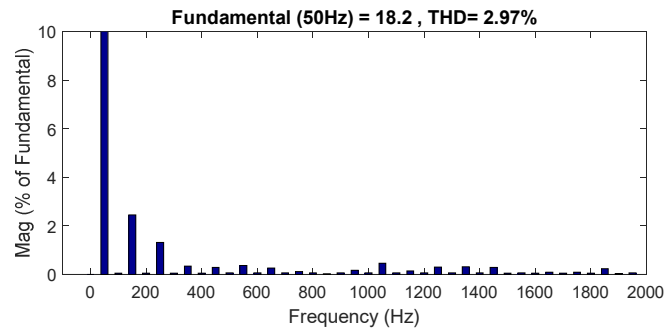


Figure 6. Spectrum of the electrical grid's current.

The Fast Terminal Sliding Mode Control – Direct Power Control strategy is also evaluated in transient conditions. The results are plotted in figure 7 and figure 8 with from to bottom, the active power, the reactive power, the electrical grid's voltage and current.

Figure 7 corresponds to solar radiation step changes ($600-1000-750W/m^2$). The results show the controller's fast response for power tracking with almost no overshoot and a null steady-state error.

Figure 8 corresponds to reactive power step changes. The results show a time response $t_r = 8\text{ms}$ for reactive power tracking with almost no overshoot and a null steady-state error.

In both cases, one can notice the good decoupling between the two power loops and the fast transient response for the electrical grid's current.

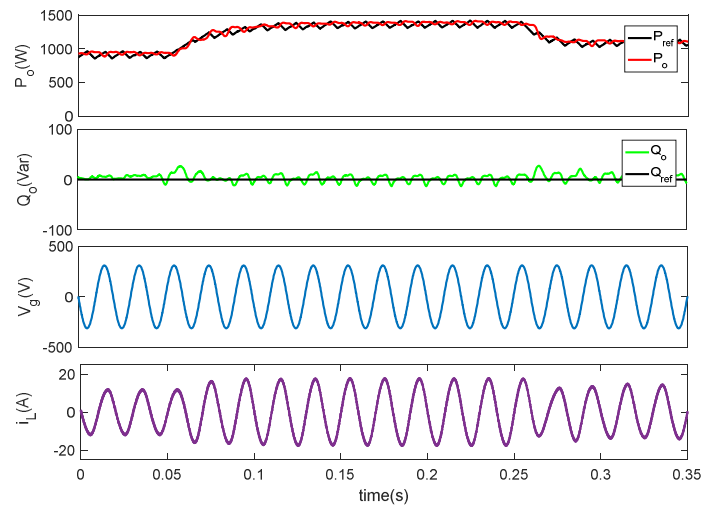


Figure 7. Simulation results of FTSMC-DPC with active power step changes.

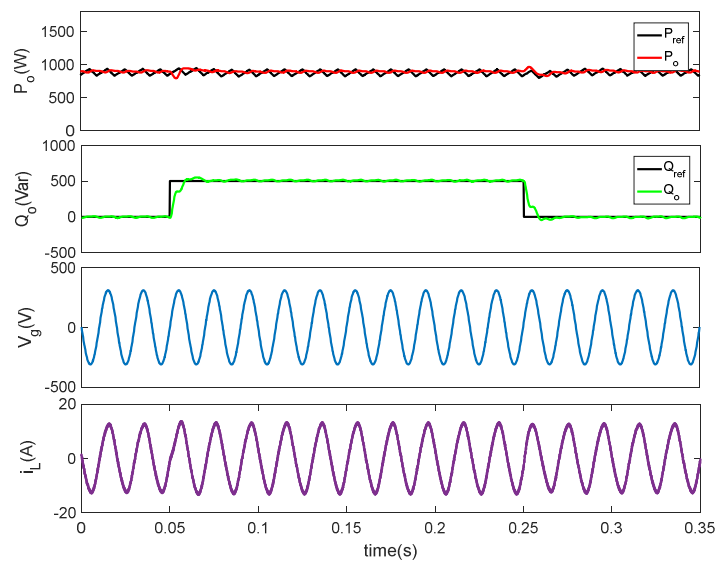


Figure 8. Simulation results of FTSMC-DPC with reactive power step changes.

2- Experimental results

The experimental testbed is shown in figure 9. An adjustable DC source fed from a 3-phase rectifier is used to emulate the PV source and its MPPT algorithm. The single-stage inverter is composed of IGBT power switches IKW40N120H3 (40A/1200V) driven with HCPL3120 optocoupler gate drivers. The control algorithm is implemented in the TMS320F28335, a DSP from TI. It offers a high-resolution enhanced pulse width modulator and high-speed analog to digital converters. Hall effect sensors, LTS25NP and LV25P are used to measure the current and the voltage, respectively.

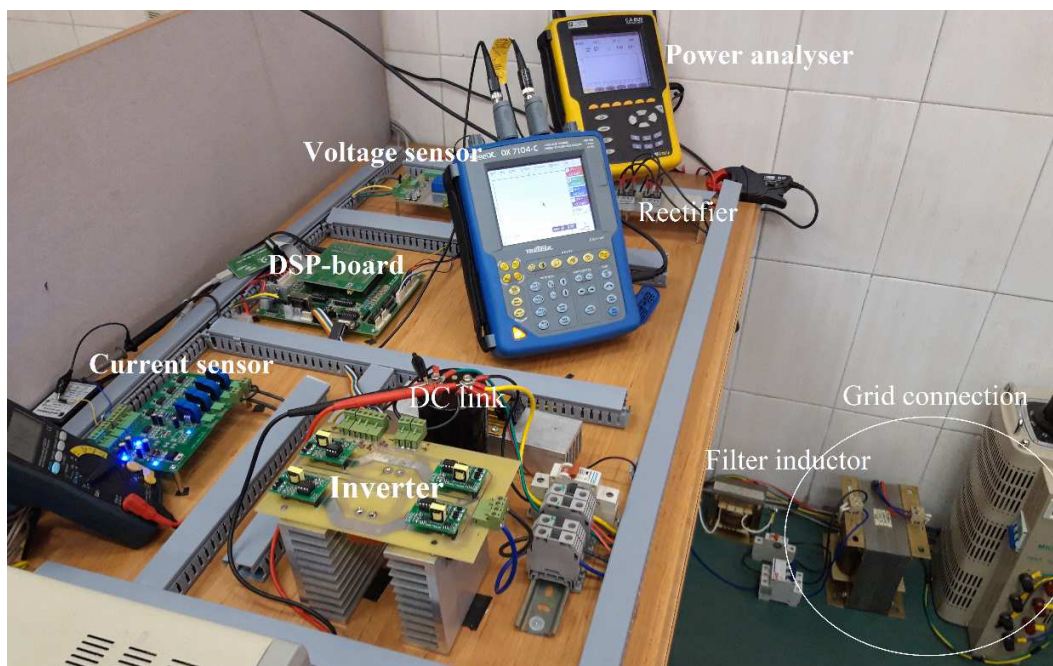


Figure 9. The experimental setup.

The experimental results in steady-state are displayed in figure 10. The active power is equal to 1kW while the reactive power is very low. One can also notice the sinusoidal waveforms of the

electrical grid's voltage and current. Figure 11 represents the current's spectrum. It shows a THD equal to 3.5% compliant with the international standard.

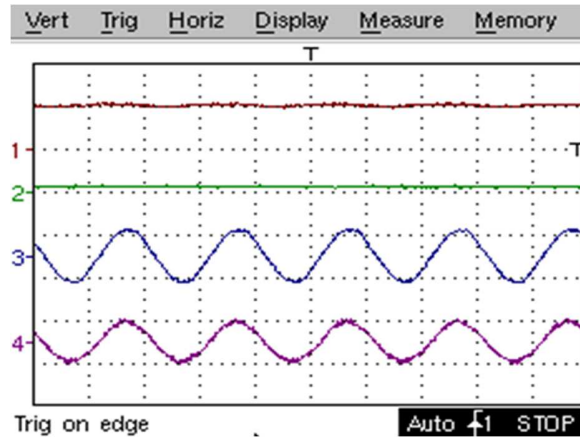


Figure 10. Experimental results of FTSMC in steady-state condition; time: (10ms/div), CH1: active power (1000 W/div), CH2: reactive power (500 VAR/div), CH3: grid voltage (500V/div), and CH4: grid current (26A/div).

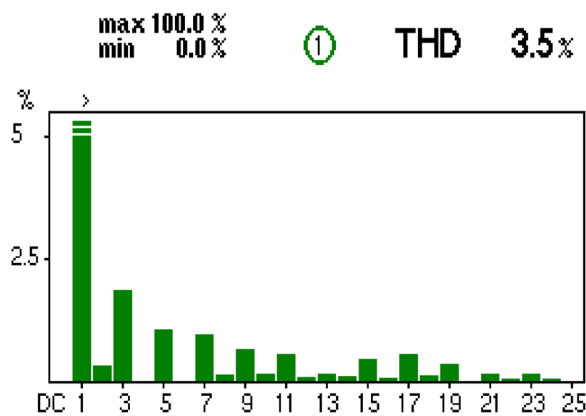


Figure 11. Grid current's spectrum in the experimental system.

The controllers' performances in case of solar radiation changes due, for example to clouds, are evaluated with active power reference stepwise variations from 50% to 100% and back to 50% of the nominal value. The results are plotted in figure 12. The power tracking performances are

very good, with almost no overshoot and time response of 10 ms. The transient on the grid's current is negligible, and there is no perturbation in the grid's voltage.

The controller is also evaluated in case of reactive power changes due to grid requirements. The results are plotted in figure 13. As for the active power regulation the same conclusions can be drawn.

Moreover, the performances during transients are better than those obtained with other methods [28-30]. From the previous results, one can also notice the good decoupling capability of the proposed controller. The two power loops (active and reactive) are almost independently controlled.

A change of $\pm 25\%$ in the inductance value is introduced in the model to verify the robustness of the proposed controller. The results plotted in figure 14 show a good robustness with a THD of the grid current equal to 3.7% compared to 3.5% when there is no parameter mismatch. The dynamics of power regulation are unchanged.

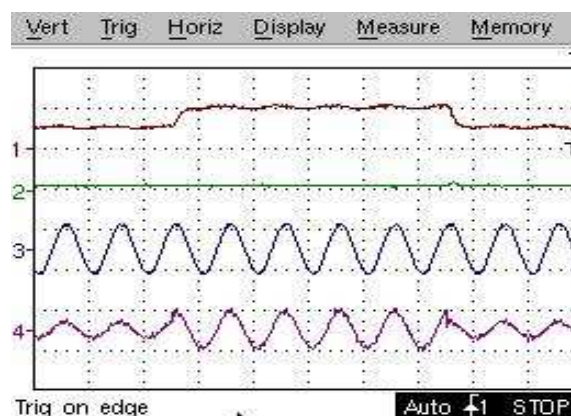


Figure 12. Experimental results of FTSMC with active power step changes; time: (20ms/div), CH1: active power (1000 W/div), CH2: reactive power (500 VAR/div), CH3: grid voltage (500V/div), and CH4: grid current (26A/div).

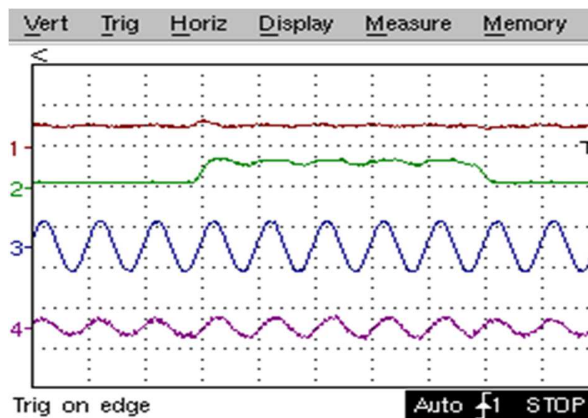


Figure 13. Experimental results of FTSMC with reactive power step changes; time: (20ms/div), CH1: active power (1000 W/div), CH2: reactive power (500 VAR/div), CH3: grid voltage (500V/div), and CH4: grid current (26A/div).

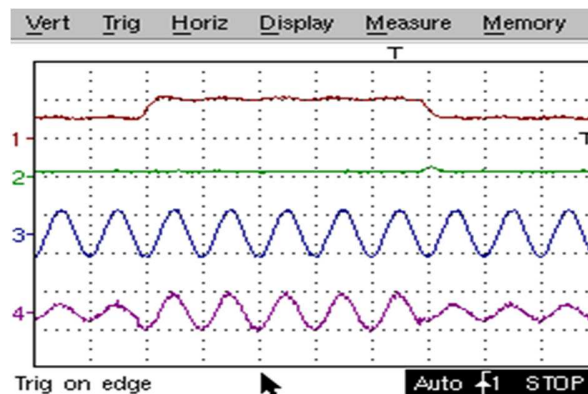


Figure 14. Experimental results of FTSMC with mismatches in filter inductor; time: (20ms/div), CH1: active power (1000 W/div), CH2: reactive power (500 VAR/div), CH3: grid voltage (500V/div), and CH4: grid current (26A/div).

Finally, a comparison of experimental results is done with a deadbeat-Direct Power Control method [29], a deadbeat predictive controller [30], and a power hysteresis control scheme with dynamic performance improvement [28]. **The main parameters and comparative results are summarized in Table 4.** We can particularly notice a lower THD for the electrical grid's current for our method. To compare the dynamic performance while the rate of active power variation is

different, we have computed the relative time response defined as $\frac{t_r}{\Delta P \%}$. The results show that our proposal exhibits the best performance.

Table 4. Experimental parameters and comparative data

Reference	Proposed DPC	[29]	[28]	[30]
Point of common coupling (PCC) voltage (V)	110	70	110	60
S_o (kVA)	1	1	1	0.5
f_{sw} (kHz)	6	5	5	2.5
$f_{sampling}$ (kHz)	12	5	-	5
Filter inductor (mH)	3.25	3.7	5.6	5
$\frac{t_r}{\Delta P \%}$ (ms)	0.1	2	0.4	0.4
Grid current THD (%)	3.5	3.9	6.81	4.63

Conclusion

In this paper, a fast terminal sliding mode control combined with a direct power controller has been designed for the control of a single-stage single-phase PV grid-connected system. Fast Terminal Sliding Mode Control has the inherent robustness of sliding mode control but has better performances in terms of quick convergence time, whatever the initial point. We have presented how the controller should be designed to mitigate the chattering phenomenon and reject the disturbances. This hybrid controller has been evaluated in simulation and in an experimental testbed in which the PV module is emulated with a DC source. The combination with direct power control has allowed to decoupling regulation of active and reactive powers even in the

presence of external perturbations. Moreover, this hybrid controller, with a fast dynamic response (less than half a cycle of the grid period), leads to a total harmonic distortion of 3.5% (compliant with the 5% of the international standard) of the current flowing into the electrical grid. The experimental results have shown that the controller is robust to input change and to the inductor' parameter mismatch. Compared with other conventional methods (deadbeat direct power control, deadbeat predictive control, hysteresis power control), it has shown lower relative time response and lower THD (better power quality).

References

- [1] U. Eia, "The international energy outlook 2016," 2017.
- [2] M. R. Isalāma, Y. Guo, and J. Zhu, *Power converters for medium voltage networks*. Springer, 2014.
- [3] K. Alluhaybi, I. Batarseh, H. Hu, and X. Chen, "Comprehensive Review and Comparison of Single-Phase Grid-Tied Photovoltaic Microinverters," *IEEE Journal of Emerging and Selected Topics in Power Electronics*, 2019.
- [4] T.-F. Wu, C.-H. Chang, L.-C. Lin, and C.-L. Kuo, "Power loss comparison of single-and two-stage grid-connected photovoltaic systems," *IEEE Transactions on Energy Conversion*, vol. 26, no. 2, pp. 707-715, 2011.
- [5] J. Ahmed and Z. Salam, "An improved perturb and observe (P&O) maximum power point tracking (MPPT) algorithm for higher efficiency," *Applied Energy*, vol. 150, pp. 97-108, 2015.
- [6] K. Ishaque, Z. Salam, and G. Lauss, "The performance of perturb and observe and incremental conductance maximum power point tracking method under dynamic weather conditions," *Applied Energy*, vol. 119, pp. 228-236, 2014.
- [7] A. K. Podder, N. K. Roy, and H. R. Pota, "MPPT methods for solar PV systems: a critical review based on tracking nature," *IET Renewable Power Generation*, 2019.
- [8] Z. Salam, J. Ahmed, and B. S. Merugu, "The application of soft computing methods for MPPT of PV system: A technological and status review," *Applied Energy*, vol. 107, pp. 135-148, 2013.
- [9] M. Aourir, A. Abouloifa, I. Lachkar, C. Aouadi, F. Giri, and J. M. Guerrero, "Non-linear control and stability analysis of single stage grid-connected photovoltaic systems," *International Journal of Electrical Power & Energy Systems*, vol. 115, p. 105439, 2020.
- [10] Y. Gui, X. Wang, H. Wu, and F. Blåbjerg, "Voltage Modulated Direct Power Control for a Weak Grid-Connected Voltage Source Inverters," *IEEE Transactions on Power Electronics*, 2019.
- [11] A. M. Howlader, S. Sadoyama, L. R. Roose, and Y. Chen, "Active power control to mitigate voltage and frequency deviations for the smart grid using smart PV inverters," *Applied Energy*, vol. 258, p. 114000, 2020.
- [12] L. Shang, D. Sun, and J. Hu, "Sliding-mode-based direct power control of grid-connected voltage-sourced inverters under unbalanced network conditions," *IET power electronics*, vol. 4, no. 5, pp. 570-579, 2011.
- [13] E. Heydari, M. Rafiee, and M. Pichan, "Fuzzy-Genetic Algorithm-Based Direct Power Control Strategy for DFIG," (in eng), *Iranian Journal of Electrical and Electronic Engineering*, Research Paper vol. 14, no. 4, pp. 353-361, 2018.
- [14] M. Pichan, H. Rastegar, and M. Monfared, "Two fuzzy-based direct power control strategies for doubly-fed induction generators in wind energy conversion systems," *Energy*, vol. 51, pp. 154-162, 2013.
- [15] J. Hu, L. Shang, Y. He, and Z. Zhu, "Direct active and reactive power regulation of grid-connected DC/AC converters using sliding mode control approach," *IEEE transactions on power electronics*, vol. 26, no. 1, pp. 210-222, 2010.

- [16] I.-S. Kim, "Sliding mode controller for the single-phase grid-connected photovoltaic system," *Applied Energy*, vol. 83, no. 10, pp. 1101-1115, 2006.
- [17] L. Hu *et al.*, "Sliding mode extremum seeking control based on improved invasive weed optimization for MPPT in wind energy conversion system," *Applied energy*, vol. 248, pp. 567-575, 2019.
- [18] M. Pichan and H. Rastegar, "Sliding-mode control of four-leg inverter with fixed switching frequency for uninterruptible power supply applications," *IEEE Transactions on industrial electronics*, vol. 64, no. 8, pp. 6805-6814, 2017.
- [19] M. Zhihong, A. P. Paplinski, and H. R. Wu, "A robust MIMO terminal sliding mode control scheme for rigid robotic manipulators," *IEEE transactions on automatic control*, vol. 39, no. 12, pp. 2464-2469, 1994.
- [20] S. K. Gudey and R. Gupta, "Recursive fast terminal sliding mode control in voltage source inverter for a low-voltage microgrid system," *IET Generation, Transmission & Distribution*, vol. 10, no. 7, pp. 1536-1543, 2016.
- [21] X. Yu and M. Zhihong, "Fast terminal sliding-mode control design for non-linear dynamical systems," *IEEE Transactions on Circuits and Systems I: Fundamental Theory and Applications*, vol. 49, no. 2, pp. 261-264, 2002.
- [22] X. Yu, M. Zhihong, and Y. Wu, "Terminal sliding modes with fast transient performance," in *Proceedings of the 36th IEEE Conference on Decision and Control*, 1997, vol. 2, pp. 962-963: IEEE.
- [23] E. Heydari and A. Y. Varjani, "Combined modified P&O algorithm with improved direct power control method applied to single-stage three-phase grid-connected PV system," in *2018 9th Annual Power Electronics, Drives Systems and Technologies Conference (PEDSTC)*, 2018, pp. 347-351: IEEE.
- [24] M. Ciobotaru, R. Teodorescu, and F. Blaabjerg, "A new single-phase PLL structure based on second order generalized integrator," in *2006 37th IEEE Power Electronics Specialists Conference*, 2006, pp. 1-6: IEEE.
- [25] V. I. Utkin, *Sliding modes in control and optimization*. Springer Science & Business Media, 2013.
- [26] J.-J. E. Slotine and W. Li, *Applied non-linear control* (no. 1). Prentice hall Englewood Cliffs, NJ, 1991.
- [27] M. Pichan, A. A. Ahamad, A. Arishamifar, and M. E. Jamarani, "A Straightforward Procedure to Select Passive Elements in Single-phase Pulse-width Modulation Rectifiers with Developed Resonant Current Controller," *Electric Power Components and Systems*, vol. 44, no. 4, pp. 379-389, 2016.
- [28] B. Liu, W. Song, J. Ma, X. Feng, and W. Li, "Dynamic performance improvement of single-phase PWM converters with power hysteresis control scheme," *IET Power Electronics*, vol. 11, no. 12, pp. 1894-1902, 2018.
- [29] M. Monfared, M. Sanatkar, and S. Golestan, "Direct active and reactive power control of single-phase grid-tie converters," *IET Power Electronics*, vol. 5, no. 8, pp. 1544-1550, 2012.
- [30] W. Song, J. Ma, L. Zhou, and X. Feng, "Deadbeat predictive power control of single-phase three-level neutral-point-clamped converters using space-vector modulation for electric railway traction," *IEEE Transactions on power electronics*, vol. 31, no. 1, pp. 721-732, 2015.